

Well-Structured Narrow Near-Infrared Absorption Based on Nonaggregated Hexarylene-Bisimide toward a Colorless Dye

Published as part of *The Journal of Organic Chemistry* special issue “Physical Organic Chemistry: Never Out of Style”.

Shoko Yoshida, Nozomi Kasakura, Miho Hirakawa, Hirofumi Morimoto, Kyohei Matsuo, Hironobu Hayashi, Mitsuaki Yamauchi, Ryutarou Kanamori, Soji Shimizu,* Hiroko Yamada,* and Naoki Aratani*



Cite This: *J. Org. Chem.* 2025, 90, 15489–15494



Read Online

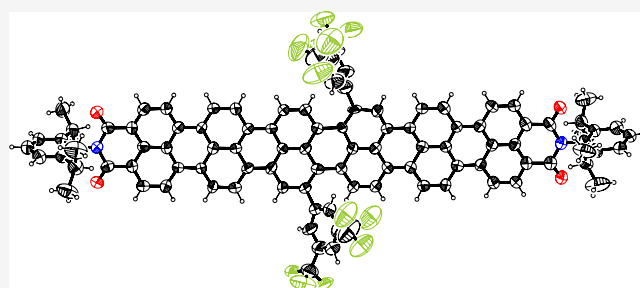
ACCESS |

Metrics & More

Article Recommendations

Supporting Information

ABSTRACT: Extended π -conjugated systems are often insoluble, and their aggregation manner greatly affects their absorption spectra. This study produced a planar, soluble, and nonaggregated hexarylene-bisimide (HB) with appropriate substituents. The single-crystal X-ray structure of HB confirmed the planar molecular structure with small twist angles and the dimerization behavior of HB in the solid state. The concentration-dependent ^1H NMR experiments in CDCl_3 indicated that the association constant K_{dimer} is $4.6 \times 10^3 \text{ M}^{-1}$ at 298 K and $\Delta G_{\text{dimer}} (298 \text{ K}) = -20.8 \text{ kJ mol}^{-1}$. The longest absorption of HB at the monomeric state exhibits a sharp and intense peak at 921 nm ($\epsilon = 230,000 \text{ M}^{-1} \text{ cm}^{-1}$, full width at half-maximum = 718 cm^{-1}) in toluene. 75% of the absorption of HB above 400 nm appears in the near-infrared region, thus giving a practically colorless solution. Magnetic circular dichroism spectra of a series of oligorylene-bisimides reveal the predominant contribution of the linear polyene-like conjugation over the annulene-like conjugation for larger $[n]$ oligorylene-bisimides.



INTRODUCTION

$[n]$ Oligorylene is one of the representative polycyclic aromatic hydrocarbons (PAHs) in which naphthalenes are linked at 1,8-positions to extend the π -conjugated system in a one-dimensional direction (Chart 1).¹ Compared to higher acenes, the chemical stability of oligorylenes is remarkably high.² The absorption spectra of $[n]$ oligorylenes exhibit a red-shift due to the effective π -conjugation and the reduction of the HOMO–LUMO gap as the number of n increases. As a result, hexarylene and higher are to be near-infrared (NIR) absorbing dyes.³ NIR absorbing dyes are applied in various fields such as optical filters, security marking, etc.⁴ For these applications, it is important to have a large absorption coefficient (ϵ) in the NIR region (750–1100 nm) with no absorption in the visible region (380–750 nm), which makes the dye colorless, selectively NIR absorbent. Nevertheless, the properties of $[n]$ oligorylenes with $n \geq 4$ have rarely been investigated, because their solubility decreases with increasing molecular length, making their synthesis and purification more challenging.² Therefore, in general, the bay-bridge alkylation⁵ and the bay-area aryloxylation⁶ have been performed to ensure the solubility and to extend the molecular length of $[n]$ oligorylenes. However, introducing the solubilizing groups into the core skeleton intrinsically broadens their absorption

spectra due to the distortion of the backbone of the oligorylenes or strong aggregation behavior by the van der Waals interaction between long alkyl chains.^{5,6}

$[n]$ Oligorylene-bisimides have electron-withdrawing imide groups with chemical stability and n -type semiconductive properties (Chart 1). The absorption spectra of the long $[n]$ oligorylene-bisimides are also broadened due to strong aggregation behavior and molecular distortion.⁷ Consequently, the absorption spectra significantly change from those of the pristine $[n]$ oligorylene-bisimides. The aggregation-free $[n]$ -oligorylene-bisimides with an undistorted skeleton should have sharper absorption spectra by suppressing the structural fluctuations.^{8,9} Currently, the longest $[n]$ oligorylene-bisimide ever synthesized without distortion of the backbone by substituents is octarylene-bisimide ($n = 8$), the molecular structure of which was confirmed only by scanning tunneling microscopy because of its strong aggregation behavior.¹⁰

Received: May 31, 2025

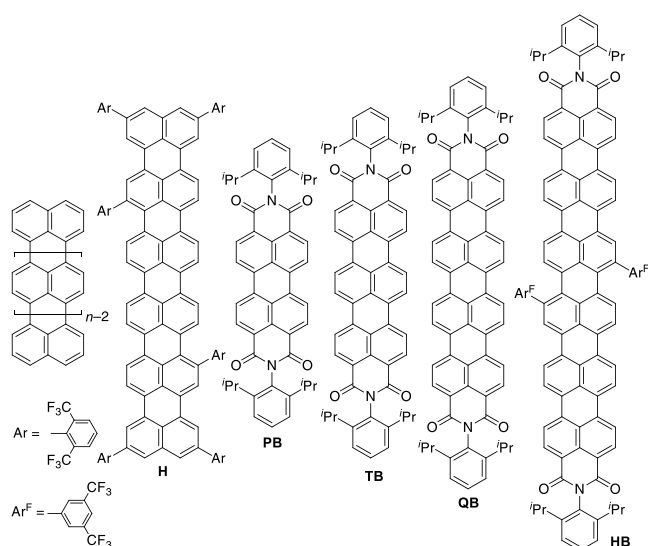
Revised: September 22, 2025

Accepted: October 17, 2025

Published: October 27, 2025



Chart 1. Chemical Structures of Oligorylenes, Hexaaryl-Hexarylene (H), and Oligorylene-Bisimides (PB–HB) in This Study



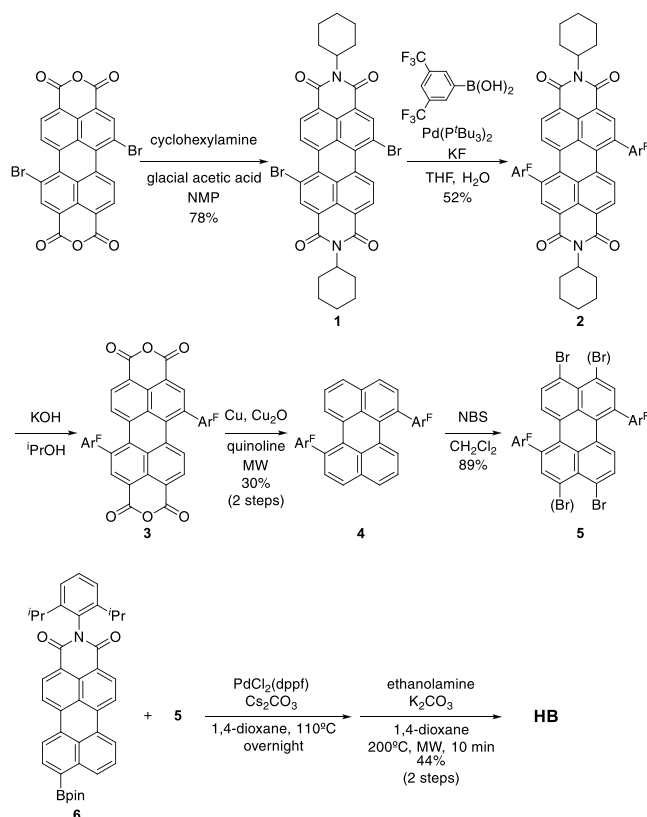
Müllen^{11a} and Langhals^{11b} also prepared planar hexarylene-bisimides (HBs), while the measurements of ¹H NMR spectra were unsuccessful due to the same reason. The objective of this study is to establish a synthetic route to undistorted soluble **HB** fused with six naphthalene units and to seek an authentic absorption spectrum of the **HB**. To prevent the distortion and to enhance the solubility at the same time, previously we prepared 2,6-bis-trifluoromethylphenyl-installed hexarylene (**H**, in Chart 1) and achieved a sharp absorption spectrum in the NIR region (831 nm in toluene, full width at half-maximum (fwhm) = 660 cm^{−1}, ϵ = 131,000 M^{−1} cm^{−1}).^{3b} In this study, electron-withdrawing, sterically hindered 3,5-bis(trifluoromethyl)phenyl groups are installed into the central bay area of the molecule. We expected that the electron-withdrawing groups stabilize the HOMO level, while the steric hindrance prevents intermolecular π - π stacking, achieving high solubility and stability. As revealed in this study, the distortion of the molecular skeleton of **HB** due to the central aryl groups is as small as 0.14° in the energy-minimized structure, resulting in the sharp absorption in the NIR region at 921 nm in toluene. On the other hand, we found that **HB** forms a discrete dimer under highly concentrated conditions, which was proved by spectroscopic and X-ray crystallographic analysis.

When the π -conjugation on the high-symmetry framework extends in one direction, the perfectly allowed transition to the first excited state ($S_0 \rightarrow S_1$) in the NIR region will result in the fairly forbidden transition to the second excited state ($S_0 \rightarrow S_2$) in the visible region so that the compound should be colorless. For this purpose, the sharpness of absorption bands is also a noticeable key issue.

RESULTS AND DISCUSSION

The original synthetic route of a **HB** was developed by Müllen and co-workers.^{11a} We slightly modified the conditions to improve the yield of **HB** as shown in Scheme 1. Pure 1,7-dibromo-3,4,9,10-perylenetetracarboxylic dianhydride¹² was transformed into bisimide **1** with cyclohexylamine in 78% yield. **1** and 3,5-bis(trifluoromethyl)phenyl boronic acid were coupled by the Suzuki–Miyaura cross-coupling reaction in 52% yield. Hydrolysis and decarboxylation reactions of **2** were

Scheme 1. Synthetic Route of Hexarylene-Bisimide **HB**



^aAr^F = 3,5-bis(trifluoromethyl)phenyl.

performed to afford 1,7-disubstituted perylene **4** in 30% yield in 2 steps.^{6a} This perylene **4** was brominated with 2 equiv of NBS to afford dibromoperylene **5** as a mixture of regioisomers in 89% yield. The Suzuki–Miyaura cross-coupling reaction of **5** with 9-borylated perylene monoimide **6**¹³ gave a perylene triad in moderate yield. Hence, the reductive fusion reaction of the triad was explored.¹¹ To our delight, the treatment of the triad in ethanolamine in the presence of K₂CO₃ at 200 °C with microwave (MW) for 10 min led to the formation of fusion product **HB** in 44% yield after purification by silica gel chromatography.

The structure of **HB** was confirmed by high-resolution matrix-assisted-laser-desorption/ionization time-of-flight (HR-MALDI-tof) mass spectrometry and ¹H- and ¹³C NMR spectroscopy. HR-MALDI-tof mass spectrometry detected the parent ion peak at m/z = 1630.4514 (calcd. for C₁₀₄H₆₂N₂O₄F₁₂ = 1630.4512 [M]⁺).

The ¹H NMR spectrum of **HB** in CDCl₃ shows well-dissolved peaks at room temperature. Variable temperature ¹H NMR measurements gave slightly sharper peaks at 50 °C than those at room temperature. The ¹H NMR spectrum consists of one singlet peak and ten doublet peaks for hexarylene protons, assigned by 2D-NMR (Supporting Information Figure S10). The proton peaks near the central unit, which were slightly broad at room temperature, became sharper with increasing temperature. This would be because the structural relaxation induced by heating is the largest in the central area (vide infra).

The single crystals suitable for X-ray diffraction analysis were obtained by vapor diffusion of methanol into a solution of **HB** in toluene (Figures 1 and S23).¹⁴ In the crystal, two independent **HB** molecules are present in the unit cell, stacked

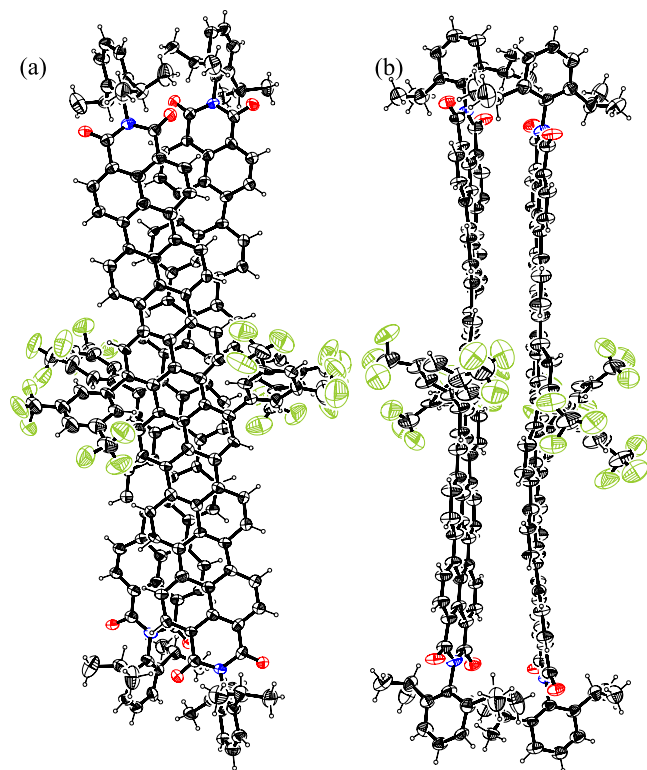


Figure 1. Single-crystal X-ray structure of **HB**. (a) Top view and (b) side view. Thermal ellipsoids are scaled at the 50% probability. Solvent molecules have been omitted for the sake of clarity.

parallel to the long axis with a mean-plane distance of 3.4 Å (Figure 1b). The hexarylene core is planar, with mean-plane deviations of 0.188 and 0.200 Å. The central core units are slightly tilted with dihedral angles of 14° and 23°. The optimized structure of **HB** calculated by density functional theory (DFT) (substituents on N atoms were replaced by hydrogen atoms) is nearly planar with a twist dihedral angle of 0.14° at the center, as expected (Figure S26). These results indicate that **HB** exhibits some flexibility due to packing effects in the crystal. As the outward-facing aryl groups become hindered, this twisting is expected to restrict π -stack association up to dimerization, even if it is possible.

Evidence of dimerization even in solution was obtained from electrospray ionization (ESI) mass spectrometry measurements of **HB**. As a result, dimer peaks were observed at $m/z = 3285.80676$ (calcd. for $C_{208}H_{124}N_4O_8F_{24}Na = 3285.8995$ [$2M + Na$] $^+$) (Figure S22). To check the dimerization behavior of **HB** in the solution state, a concentration-dependent chemical shift of **HB** in $CDCl_3$ was traced via 1H NMR measurements. As an example, the chemical shift profiles of the proton peaks at 298 K are illustrated in Figure 2: the proton peaks originally observed at 8.06, 8.22, and 8.56 ppm were shifted to upfield at 8.02, 8.03, and 8.30 ppm, respectively, due to the dimerization. The spectral features are analogous to those of other supramolecular systems.¹⁵ These dimerization profiles (8 samples, total data points $N = 24$) were analyzed with the curve-fitting for binding systems (Figures S11–S16 and Tables S1–S3).¹⁶ Assuming that the dimer is in equilibrium, the equilibrium constants (K_{dimer}) were estimated to be 4.6, 2.1, and $1.6 \times 10^3 M^{-1}$ at 298, 318, and 328 K, respectively. The thermodynamic parameters (ΔH , ΔS , and ΔG_{dimer} (298 K)) were estimated at $-27.4 kJ mol^{-1}$, $-22 J K^{-1} mol$, and -20.8

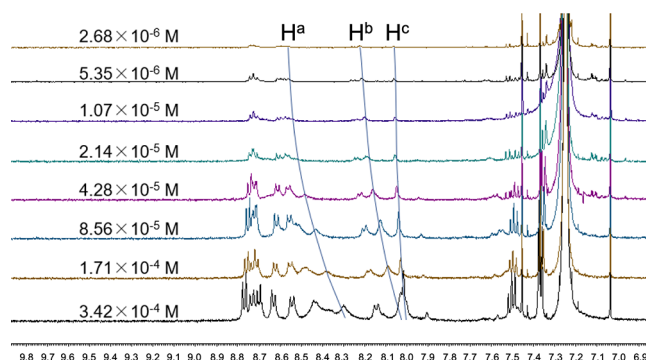


Figure 2. Concentration-dependent 1H NMR spectra (500 MHz) of **HB** in $CDCl_3$ at 298 K.

$kJ mol^{-1}$, respectively, from the van't Hoff plots. From these values, it is clear that the dominant formation of the dimer in the equilibrium is attributable to the larger enthalpy term ($T\Delta S < \Delta H$).

The dimeric architecture of **HB** was further corroborated by diffusion-ordered 2D-NMR spectroscopy (DOSY) in $CDCl_3$. The 1H NMR signal at 2.8 ppm was with a diffusion coefficient (D) at $3.63 \times 10^{-10} m^2/s$ at $[HB] = 7.3 \times 10^{-4} M^{-1}$, which is comparable to that of the bilayer nanographene¹⁷ ($M_w = 3829.49$, $D = 2.17 \times 10^{-10} m^2/s$), suggesting the comparable molecular weight. It should be noted that unlike bilayer nanographene, which clearly forms a dimer in solution, **HB** exists in equilibrium between monomer and dimer in solution.

The absorption spectrum of **HB** along with perylene-bisimide **PB**, terrylene-bisimide **TB**, quaterylene-bisimide **QB**, and hexarylene **H** in toluene is shown in Figure 3. As expected, the maximum absorption wavelength was observed at 921 nm, and the molar absorption coefficient was $2.30 \times 10^5 M^{-1} cm^{-1}$ with an fwhm of $718 cm^{-1}$. The second and third vibrational bands of the first electronic transition also have absorption bands in the NIR region (818 and 740 nm), indicating that the compound could be colorless in the solvent. 75% of the absorption of **HB** above 400 nm appears in the NIR region. By comparing the absorption spectrum of **HB** with those of other [2]–[4]oligorylene-bisimides, it was experimentally revealed that the absorption wavenumber ($S_0 \rightarrow S_1$) becomes smaller proportional to the inverse of the molecular length and that the effective conjugation length (ECL) continues to extend without saturation at least up to **HB** (Figure S25), as in oligorylenes.^{3b} Since the plot of the energy gap versus the inverse of the number of repeating units is perfectly linear, we consider an ideal model to be an electron in a one-dimensional box.¹¹ Very interestingly, the intercepts are the same for oligorylene and oligorylene-bisimide ($\sim 7,000 cm^{-1}$, 0.87 eV). This could indicate the intrinsic band gap of graphene nanoribbons ([5]GNRs), which is not affected by the substrate surfaces.¹⁸ The steady-state fluorescence of **HB** was not observed like hexarylene.^{3b}

Cyclic voltammetry (CV) measurements in CH_2Cl_2 were performed to investigate the redox properties of a series of oligorylene-bisimides. The working, counter, and reference electrodes are glassy carbon, Pt wire, and $Ag/AgNO_3$, respectively. With 0.1 M nBu_4NPF_6 as the electrolyte, the potentials were determined based on the ferrocene/ferrocenium (Fc/Fc^+) couple. The results and values compared to those of oligorylenebisimides are summarized in Figure 4 and Table S5. Reversible oxidation and reduction waves were

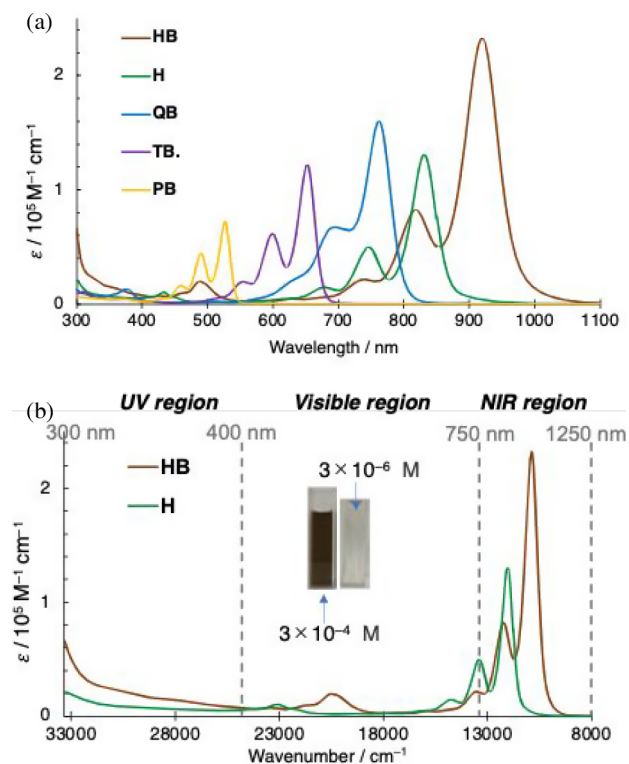


Figure 3. (a) UV-vis-NIR absorption spectra of a series of oligorylene-bisimides in toluene in wavelength unit. $[HB] = 2.4 \times 10^{-7} \text{ M}$. (b) UV-vis-NIR absorption spectra of **H** and **HB** in wavenumber unit. The inset shows photographs of **HB** solutions.

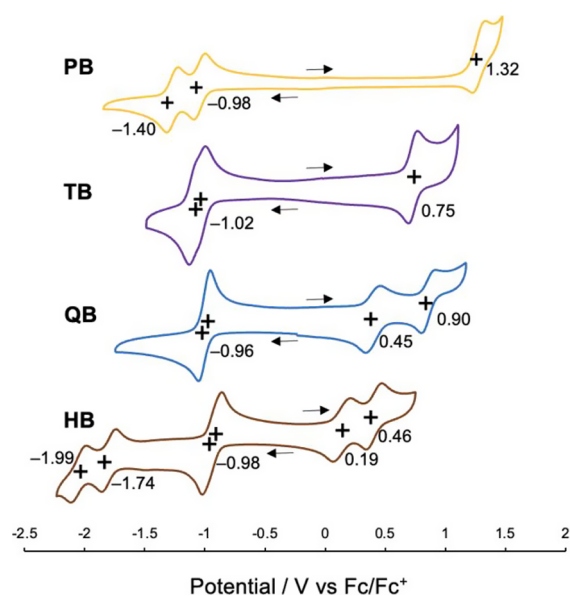


Figure 4. Cyclic voltammogram of a series of oligorylene-bisimide in CH_2Cl_2 (IUPAC convention). $[HB] = 6.0 \times 10^{-5} \text{ M}$. The working, counter, and reference electrodes are glassy carbon, Pt wire, and Ag/AgNO_3 , respectively. With $0.1 \text{ M } n\text{Bu}_4\text{NPF}_6$ as the electrolyte, the potentials were determined based on the ferrocene/ferrocenium (Fc/Fc^+) couple.

observed at 1.32, -0.98 , and -1.40 V for **PB**, at 0.75 and -1.02 ($2e^-$) V for **TB**, at 0.90 , 0.45 , and -0.96 ($2e^-$) V for **QB**, and 0.46 , 0.19 , -0.98 ($2e^-$), -1.74 and -1.99 V for **HB**, respectively. While the first oxidation potential (E_{ox1}) shifts to the negative side with the elongation of the molecular length,

the first reduction potential (E_{red1}) remains unchanged for all oligorylenebisimides (ca. -1.0 V), and the two-electron reduction occurs for higher oligorylene-bisimides. Thus, the difference in redox potentials ($E_{\text{ox1}} - E_{\text{red1}}$) eventually decreased as the molecular length became longer. These results suggest that the oxidation is initiated at the center of the molecule, while the reduction occurs at the imide moieties at both ends. These features showed good agreement with the calculated electronic structures (Figure S24).

To further give a detailed insight into the electronic structures of a series of $[n]$ oligorylene-bisimides, magnetic circular dichroism (MCD) spectra were measured (Figure 5).¹⁹ **PB** exhibits the characteristic MCD signals as a perylene-

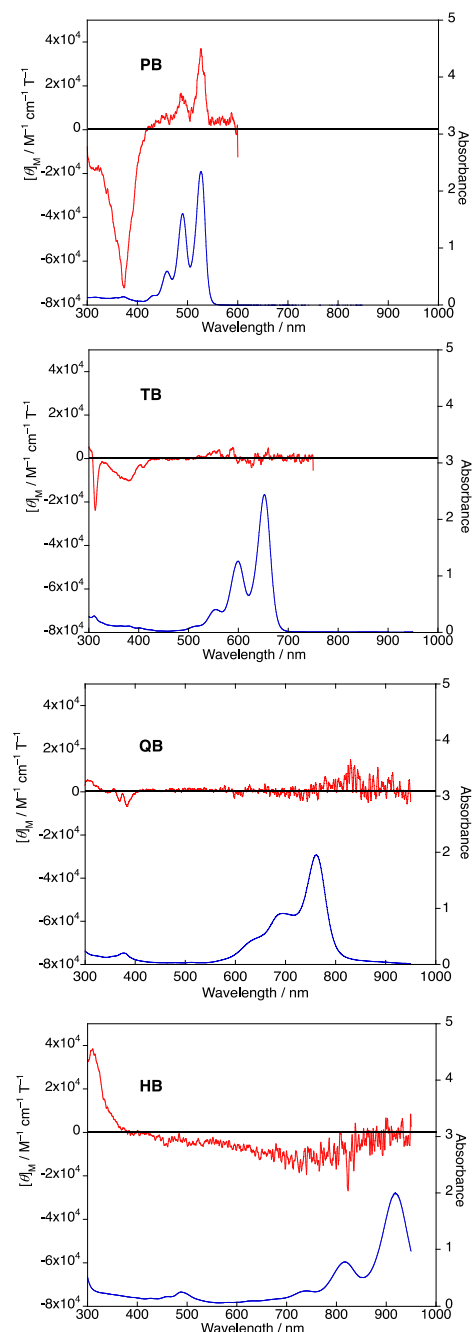


Figure 5. MCD and absorption spectra of a series of oligorylene-bisimides in CH_2Cl_2 .

bisimide derivative,²⁰ a relatively weak positive Faraday *B* term corresponding to the S_0 -to- S_1 transition, followed by an intense negative Faraday *B* term around 375 nm. In contrast to the intensification of the S_0 -to- S_1 transition in the order **PB**, **TB**, **QB**, and **HB**, the corresponding MCD signals become less significant in the same order and are nearly diminished in the case of **HB**. The MCD signals arise from the Faraday effect due to the interaction between the applied magnetic field and the magnetic dipole moments associated with the orbital motion of electrons, which is mainly contributed by the annulene-like conjugation in the current case. The weaker MCD signals observed for the larger [*n*]oligorylene-bisimides, therefore, indicate the more significant contribution of the linear polyene-like conjugation than the annulene-like conjugation,²¹ which can be enhanced by the planar structure with negligible distortion.

CONCLUSIONS

In summary, we successfully synthesized 10,24-bis[3,5-bis-(trifluoromethyl)phenyl]hexarylene-bisimide **HB** using a reductive fusion reaction of the perylene triad. The product is soluble in common organic solvents and could be purified with column chromatography. The optimized structure revealed that the hexarylene core is not significantly disturbed by the substituents very much and is almost planar. We have shown that **HB** is stacked and dimerized in the solid state and in high concentration solutions, but we have also shown that **HB** is monomeric under conditions where absorption spectra are measured, thus allowing us to measure the physical properties of **HB** in its discrete state. The longest absorption of **HB** exhibits a sharp peak at 921 nm in toluene with the fwhm of 718 cm^{-1} . The substituents did not perturb the electronic properties of **HB**. The molecular coefficient is as large as 230,000 $\text{M}^{-1} \text{cm}^{-1}$, and 75% of the absorption bands of **HB** appear in the NIR region. Eventually, **HB** having less absorption at the visible light region was sufficiently stable under the LED room light conditions for more than 1 week. The perfect straight line of the plots of the excitation energy and $1/n$ exhibits an ideal particle-in-a-box model. The physical properties of GNRs vary greatly depending on the edge state, length, and interaction with the substrate.¹⁷ Oligorylene-bisimide is the thinnest armchair graphene nanoribbon ([5]AGNR), which is in a discrete form with a well-defined length and substituents by solution synthesis, not on-surface synthesis, and is a valuable model for GNR. In total, we succeeded in producing the NIR dye based on oligorylene, having no absorption peaks in the visible light region, and the solution is almost colorless.

ASSOCIATED CONTENT

Data Availability Statement

The data underlying this study are available in the published article and its [Supporting Information](#).

Supporting Information

The Supporting Information is available free of charge at <https://pubs.acs.org/doi/10.1021/acs.joc.5c01320>.

Synthetic procedures, NMR, MS, UV-vis spectroscopic data, SCXRD results, and DFT calculation data ([PDF](#))

Accession Codes

Deposition Number 2439975 contains the supplementary crystallographic data for this paper. These data can be obtained free of charge via the joint Cambridge Crystallographic Data

Centre (CCDC) and Fachinformationszentrum Karlsruhe Access Structures service.

AUTHOR INFORMATION

Corresponding Authors

Soji Shimizu – Department of Applied Chemistry, Graduate School of Engineering, and Center for Molecular Systems (CMS), Kyushu University, Fukuoka 819-0395, Japan; orcid.org/0000-0002-2184-7468; Email: ssoji@cstf.kyushu-u.ac.jp

Hiroko Yamada – Institute for Chemical Research, Kyoto University, Kyoto 611-0011, Japan; orcid.org/0000-0002-2138-5902; Email: hyamada@scl.kyoto-u.ac.jp

Naoki Aratani – Division of Materials Science and Medilux Research Center, Nara Institute of Science and Technology (NAIST), Ikoma 630-0192, Japan; orcid.org/0000-0002-3181-6526; Email: aratani@ms.naist.jp

Authors

Shoko Yoshida – Division of Materials Science, Nara Institute of Science and Technology (NAIST), Ikoma 630-0192, Japan

Nozomi Kasakura – Division of Materials Science, Nara Institute of Science and Technology (NAIST), Ikoma 630-0192, Japan

Miho Hirakawa – Division of Materials Science, Nara Institute of Science and Technology (NAIST), Ikoma 630-0192, Japan

Hirofumi Morimoto – Division of Materials Science, Nara Institute of Science and Technology (NAIST), Ikoma 630-0192, Japan

Kyohei Matsuo – Institute for Chemical Research, Kyoto University, Kyoto 611-0011, Japan

Hironobu Hayashi – Center for Basic Research on Materials, National Institute for Materials Science (NIMS), Tsukuba, Ibaraki 305-0047, Japan; orcid.org/0000-0002-7872-3052

Mitsuaki Yamauchi – Institute for Chemical Research, Kyoto University, Kyoto 611-0011, Japan; orcid.org/0000-0003-0005-5960

Ryutarou Kanamori – Department of Applied Chemistry, Graduate School of Engineering, and Center for Molecular Systems (CMS), Kyushu University, Fukuoka 819-0395, Japan

Complete contact information is available at: <https://pubs.acs.org/10.1021/acs.joc.5c01320>

Author Contributions

The manuscript was written through the contributions of all authors.

Notes

The authors declare no competing financial interest.

ACKNOWLEDGMENTS

This work was supported by the Japan Society for the Promotion of Science (JSPS) KAKENHI Grant Nos. JP23K23332 (SS), JP24K01576 (HH), JP23K26480 (NA), JP25K01751 (HY), and JP20H05833 (Transformative Research Areas “Dynamic Exciton”), JST PRESTO JPMJPR21AC (HH), the CASIO SCIENCE PROMOTION FOUNDATION (J41-23) funds, and the Masuyakinen basic research foundation. We thank Yoshiko Nishikawa (NAIST)

for the MS measurements. We also thank Prof. Dr. Shohei Saito, Dr. Akito Nakai (Kyoto University), and Shohei Katao (NAIST) for their help with the X-ray analysis. This work was partly supported by the ARIM Program of the Ministry of Education, Culture, Sports, Science and Technology (MEXT) (JPMXP1225NRS003). H.M. is grateful to the NAIST Special Fund and University Fellowships for Young Scientists.

REFERENCES

- (1) (a) Markiewicz, J. T.; Wudl, F. Perylene, Oligorylenes, and Aza-Analogs. *ACS Appl. Mater. Interfaces* **2015**, *7*, 28063–28085. (b) Würthner, F.; Saha-Möller, C. R.; Fimmel, B.; Ogi, S.; Leowanawat, P.; Schmidt, D. Perylene Bisimide Dye Assemblies as Archetype Functional Supramolecular Materials. *Chem. Rev.* **2016**, *116*, 962–1052.
- (2) Chen, L.; Li, C.; Müllen, K. Beyond perylene diimides: synthesis, assembly, and function of higher rylene chromophores. *J. Mater. Chem. C* **2014**, *2*, 1938–1956.
- (3) (a) Zhao, X.; Xiong, Y.; Ma, J.; Yuan, Z. Rylene and Rylene Diimides: Comparison of Theoretical and Experimental Results and Prediction for High-Rylene Derivatives. *J. Phys. Chem. A* **2016**, *120*, 7554–7560. (b) Fujita, R.; Yoshida, S.; Kano, H.; Matsuo, K.; Hayashi, H.; Yamada, H.; Aratani, N. A Series of Soluble Planar Oligorylenes up to Hexarylene. *Chin. J. Chem.* **2023**, *41*, 1023–1027.
- (4) Qian, G.; Wang, Z. Y. Near-Infrared Organic Compounds and Emerging Applications. *Chem.-Asian J.* **2010**, *5*, 1006–1029.
- (5) (a) Li, Y.; Gao, J.; Motta, S. D.; Negri, F.; Wang, Z. Tri-N-annulated Hexarylene: An Approach to Well-Defined Graphene Nanoribbons with Large Dipoles. *J. Am. Chem. Soc.* **2010**, *132*, 4208–4213. (b) Qi, Q.; Burrezo, P. M.; Phan, H.; Herng, T. S.; Gopalakrishna, T. Y.; Zeng, W.; Ding, J.; Casado, J.; Wu, J. Ambient Stable Radical Cations, Diradicaloid π -Dimeric Dications, Closed-Shell Dications, and Diradical Dications of Methylthio-Capped Rylens. *Chem.-Eur. J.* **2017**, *23*, 7595–7606. (c) Zeng, W.; Hong, Y.; Rivero, S. M.; Kim, J.; Zafra, J. L.; Phan, H.; Gopalakrishna, T. Y.; Herng, T. S.; Ding, J.; Casado, J.; Kim, D.; Wu, J. Stable Nitrogen-Centered Bis(imino)rylene Diradicaloids. *Chem.-Eur. J.* **2018**, *24*, 4944–4951. (d) Zeng, W.; Phan, H.; Herng, T. S.; Gopalakrishna, T. Y.; Aratani, N.; Zeng, Z.; Yamada, H.; Ding, J.; Wu, J. Rylene Ribbons with Unusual Diradical Character. *Chem.* **2017**, *2*, 81–92.
- (6) (a) Former, C.; Becker, S.; Grimsdale, A. C.; Müllen, K. Cyclodehydrogenation of poly(perylenes) to poly(quaterylene)s: Toward poly(peri-naphthalene). *Macromolecules* **2002**, *35*, 1576–1582. (b) Miletić, T.; Fermi, A.; Papadakis, I.; Orfanos, I.; Karampitsos, N.; Avramopoulos, A.; Demitri, N.; Leo, F. D.; Pope, S. J. A.; Papadopoulos, M. G.; Couris, S.; Bonifazi, D. A Twisted Bay-Substituted Quaterylene Phosphorescing in the NIR Spectral Region. *Helv. Chim. Acta* **2017**, *100*, No. e1700192. (c) Nakazawa, H.; Sako, M.; Masui, Y.; Kurosaki, R.; Yamamoto, S.; Kamei, T.; Shimada, T. C–H Triflation of BINOL Derivatives Using DIH and TfOH. *Org. Lett.* **2019**, *21*, 6466–6470.
- (7) Geerts, Y.; Quante, H.; Platz, H.; Mahrt, R.; Hopmeier, M.; Böhm, A.; Müllen, K. Quaterylenebis(dicarboximide)s: near infrared absorbing and emitting dyes. *J. Mater. Chem.* **1998**, *8*, 2357–2369.
- (8) Cravencio, A.; Yu, Y.; Edhborg, F.; Goebel, J. F.; Takacs, Z.; Yang, Y.; Albinsson, B.; Björjesson, K. Exciton Delocalization Counteracts the Energy Gap: A New Pathway toward NIR-Emissive Dyes. *J. Am. Chem. Soc.* **2021**, *143*, 19232–19239.
- (9) Jiao, L.; Zou, Y.; Fan, W.; Han, Y.; Zhou, Q.; Shao, J.; Wu, J. Aggregation-Free, Highly Soluble CN-Terminated Dicyclopentadiene-Fused Rylens. *J. Am. Chem. Soc.* **2025**, *147*, 9415–9423.
- (10) Yuan, Z.; Lee, S.-L.; Chen, L.; Li, C.; Mali, K. S.; Feyter, S.; De Müllen, K. Processable Rylene Diimide Dyes up to 4 nm in Length: Synthesis and STM Visualization. *Chem.-Eur. J.* **2013**, *19*, 11842–11846.
- (11) (a) Pschirer, N. G.; Kohl, C.; Nolde, F.; Qu, J.; Müllen, K. Pentarylene- and Hexarylenebis(dicarboximide)s: Near-Infrared-Absorbing Polyaromatic Dyes. *Angew. Chem., Int. Ed.* **2006**, *45*, 1401–1404. (b) Langhals, H.; Zgela, D.; Lüling, R. Sexterylenetetra-carboxylic Bisimides: NIR Dyes. *J. Org. Chem.* **2015**, *80*, 12146–12150.
- (12) (a) Würthner, F.; Stepanenko, V.; Chen, Z.; Saha-Möller, C. R.; Kocher, N.; Stalke, N. Preparation and Characterization of Regioisomerically Pure 1,7-Disubstituted Perylene Bisimide Dyes. *J. Org. Chem.* **2004**, *69*, 7933–7939. (b) Sengupta, S. S.; Dubey, R. K.; Hoek, R. W. M.; van Eeden, S. P. P.; Deniz Gunbaş, D.; Grozema, F. C.; Sudhölter, E. J. R.; Jager, W. F. Synthesis of Regioisomerically Pure 1,7-Dibromoperylene-3,4,9,10-tetracarboxylic Acid Derivatives. *J. Org. Chem.* **2014**, *79*, 6655–6662. We purchased pure (>98.0%) 1,7-dibromo-3,4,9,10-perylenetetra-carboxylic dianhydride from TCI (Product Number: D3871).
- (13) Weil, T.; Abdalla, M. A.; Jatzke, C.; Hengstler, J.; Müllen, K. Water-Soluble Rylene Dyes as High-Performance Colorants for the Staining of Cells. *Biomacromolecules* **2005**, *6*, 68–79.
- (14) **HB**: $C_{104}H_{62}F_{12}N_2O_4 \cdot 1.5(C_7H_8)$, $M_w = 1769.75$, monoclinic, space group $C2/c$ (no. 15), $a = 42.8218(17)$, $b = 17.7341(6)$, $c = 25.1111(7)$ Å, $\beta = 110.386(4)^\circ$, $V = 17875.1(11)$ Å³, $Z = 8$, $T = 86$ K, $D_{\text{calcd}} = 1.315$ g cm⁻³, $R_1 = 0.0977$ ($I > 2\sigma(I)$), $R_w = 0.3158$ (all data), $GO_F = 1.032$. CCDC 2439975 contains the supplementary crystallographic data for this paper. These data can be obtained free of charge from The Cambridge Crystallographic Data Centre via www.ccdc.cam.ac.uk/data_request/cif.
- (15) (a) Yang, X.; Brückner, M.; Rominger, F.; Kirschbaum, T.; Mastalerz, M. Dispersion-driven formation of chiral twisted PAH double helices. *Chem.* **2024**, *10*, 832–842. (b) Mahlmeister, B.; Schembri, T.; Stepanenko, V.; Shoyama, K.; Stolte, M.; Würthner, F. Enantiopure J-Aggregate of Quaterylene Bisimides for Strong Chiroptical NIR-Response. *J. Am. Chem. Soc.* **2023**, *145*, 13302–13311.
- (16) (a) Bindfit, <http://supramolecular.org>. (b) Thordarson, P. Determining association constants from titration experiments in supramolecular chemistry. *Chem. Soc. Rev.* **2011**, *40*, 1305–1323. (c) Brynn Hibbert, D.; Thordarson, P. The death of the Job plot, transparency, open science and online tools, uncertainty estimation methods and other developments in supramolecular chemistry data analysis. *Chem. Commun.* **2016**, *52*, 12792–12805.
- (17) Qiu, Z.-L.; Cheng, Y.; Zeng, Q.; Wu, Q.; Zhao, X.-J.; Xie, R.-J.; Feng, L. B.; Liu, K.; Tan, Y. Z. Synthesis and Interlayer Assembly of a Graphenic Bowl with Peripheral Selenium Annulation. *J. Am. Chem. Soc.* **2023**, *145*, 3289–3293.
- (18) (a) Zhang, H.; Lin, H.; Sun, K.; Chen, L.; Zagranyski, Y.; Aghdassi, N.; Duhm, S.; Li, Q.; Zhong, D.; Li, Y.; Müllen, K.; Fuchs, H.; Chi, L. On-Surface Synthesis of Rylene-Type Graphene Nanoribbons. *J. Am. Chem. Soc.* **2015**, *137*, 4022–4025. (b) Kimouche, A.; Ervasti, M. M.; Drost, R.; Halonen, S.; Harju, A.; Joensuu, P. M.; Sainio, J.; Liljeroth, P. Ultra-Narrow Metallic Armchair Graphene Nanoribbons. *Nat. Commun.* **2015**, *6*, 10177. (c) Lawrence, J.; Brandimarte, P.; Berdonces-Layunta, A.; Mohammed, M. S. G.; Grewal, A.; Leon, C. C.; Sánchez-Portal, D.; de Oteyza, D. G. Probing the Magnetism of Topological End States in 5-Armchair Graphene Nanoribbons. *ACS Nano* **2020**, *14*, 4499–4508.
- (19) Kobayashi, N.; Muranaka, A.; Mack, J. *Circular Dichroism and Magnetic Circular Dichroism Spectroscopy for Organic Chemists*; Royal Society of Chemistry: UK, 2012.
- (20) Ghidinelli, S.; Fusè, M.; Mazzeo, G.; Abbate, S.; Longhi, G. MCD and Induced CD of a Tetraphenoxyperylene-Based Dye in Chiral Solvents: An Experimental and Computational Study. *Symmetry* **2022**, *14*, 1108.
- (21) Matsumoto, A.; Suzuki, M.; Hayashi, H.; Daiki Kuzuhara, D.; Yuasa, J.; Kawai, T.; Aratani, N.; Yamada, H. Studies on Pyrene and Perylene Derivatives upon Oxidation and Application to a Higher Analogue. *Bull. Chem. Soc. Jpn.* **2017**, *90*, 667–677.